Journal of Magnetic Resonance 364 (2024) 107708

Contents lists available at ScienceDirect

Journal of Magnetic Resonance

journal homepage: www.elsevier.com/locate/jmr

MAS NMR experiments of corynebacterial cell walls: Complementary ^{1}H- and CPMAS CryoProbe-enhanced ^{13}C-detected experiments

Alicia Vallet [a], Isabel Ayala [a], Barbara Perrone [b], Alia Hassan [b], Jean-Pierre Simorre [a], Catherine Bougault [a,*], Paul Schanda [c,*]

[a] Univ. Grenoble Alpes, CNRS, CEA, Institut de Biologie Structurale, 71, avenue des martyrs, Grenoble, 38000, France
[b] Bruker Biospin, Fällanden, 8117, Switzerland
[c] Institute of Science and Technology Austria, Am Campus 1, Klosterneuburg, 3400, Austria

ARTICLE INFO

Dataset link:

Keywords:
Bacterial cell wall
Corynebacteria
Proton detection
Cross polarisation
INEPT
Solid-state NMR

ABSTRACT

Bacterial cell walls are gigadalton-large cross-linked polymers with a wide range of motional amplitudes, including rather rigid as well as highly flexible parts. Magic-angle spinning NMR is a powerful method to obtain atomic-level information about intact cell walls. Here we investigate sensitivity and information content of different homonuclear ^{13}C–^{13}C and heteronuclear ^{1}H–^{15}N, ^{1}H–^{13}C and ^{15}N–^{13}C correlation experiments. We demonstrate that a CPMAS CryoProbe yields ca. 8-fold increased signal-to-noise over a room-temperature probe, or a ca. 3–4-fold larger per-mass sensitivity. The increased sensitivity allowed to obtain high-resolution spectra even on intact bacteria. Moreover, we compare resolution and sensitivity of ^{1}H MAS experiments obtained at 100 kHz vs. 55 kHz. Our study provides useful hints for choosing experiments to extract atomic-level details on cell-wall samples.

1. Introduction

The unique architecture of the bacterial cell wall [1,2], comprising a gigadalton-large peptidoglycan, sets bacteria apart from eukaryotic cells or other kingdoms of life comprising a cell wall, such as plants [3,4], algae [5] or fungi [6,7]. Due to its primordial importance for mechanical stability, efficient impermeability, and unique chemical composition, the bacterial cell wall is an important target for antimicrobial drugs [8] and inhibition of its biosynthetic assembly has been extensively studied [9]. Within the bacterial kingdom, *Corynebacteriales*, an order that includes the pathogenic *Mycobacterium tuberculosis* and the model organism *Corynebacterium glutamicum*, show the most intricate multilayered cell envelope and cell wall core [10,11] (see Fig. 1a). In these bacteria, the peptidoglycan is connected through a rhamnose-N-acetylglucosamine-1-phosphate linker to a large arabinogalactan polymer, with terminal arabinans esterified by mycolic acids. The resulting mycoloyl-arabinogalactan-peptidoglycan (mAGP) complex is characterised by a wide range of flexibility, with fairly rigid to highly disordered portions. Moreover, despite well preserved and characterised motifs, the detailed arrangement and oligosaccharidic chain length in arabinogalactans, the number of unsaturations in the mycolic acid lipidic tail, or the number and pattern of cross-links in the peptidoglycan layer vary upon environmental factors, the state of the cell and the presence of antibacterial drugs [12,13]. This heterogeneity and dynamic disorder make atomic-level studies by crystallography or electron microscopy essentially impossible. NMR is uniquely suited to study bacterial cell walls, not only on fragments obtained by biochemical fragmentation (for examples of liquid-state NMR studies in *Corynebacteriales* see [14–16]), but also on intact isolated cell walls [17–19] or cell walls in intact bacteria [12,20], as has been shown by numerous studies by several groups including ours [21,22]. Solid-state magic-angle spinning (MAS) NMR has in particular allowed to investigate cross-linking patterns and how they depend on *e.g.* antibiotic stress [23–25], quantify peptidoglycan dynamics [26,27], or study how proteins bind to the cell wall [21,28].

Various ways of recording MAS NMR spectra can be envisaged [29], and the choice of methods is often dictated by the sensitivity consideration as well as the possibility to isotopically label the sample. In amorphous non-soluble biological samples, dynamic nuclear polarization (DNP) has been proposed to overcome sensitivity limitations, allowing to collect 2D ^{13}C-^{13}C correlation spectra at natural abundance [30–32] or to detect low populations of ^{13}C,^{15}N-isotopically labelled biomolecules in highly complex environments [20,33–36] (for recent reviews on DNP applications in biological solids see for example [37–39]). (^{13}C,^{15}N)-isotopic labelling is generally very useful in more conventional solid-state NMR approaches, as the heteronuclear dimensions often provide highest resolution. With ^{13}C (and possibly

* Corresponding authors.
E-mail addresses: catherine.bougault@ibs.fr (C. Bougault), paul.schanda@ist.ac.at (P. Schanda).

https://doi.org/10.1016/j.jmr.2024.107708
Received 14 April 2024; Received in revised form 24 May 2024; Accepted 3 June 2024
Available online 6 June 2024

^{15}N) labelled samples,^{13}C detection has long been the primary method to study a variety of cell walls or extracellular matrices [40,41] from plants [42–44], algae [45], fungi [46,47], bacteria [18] or biofilms [48,49], primarily using larger-diameter rotors (*e.g.* 3.2-mm rotors) spinning at a MAS frequency ≤ 20 kHz. Resolution in ^{1}H dimensions at this rather slow spinning rate is often poor as second- and higher-order average Hamiltonian terms contribute to line widths particularly for ^{1}H, due to their stronger dipolar couplings, with the exception of dynamic averaging in highly flexible portions [50] of biological samples at natural abundance [51] or with ^{13}C,^{15}N-labelling [52]. Faster MAS, such as 50–60 kHz or ≥ 100 kHz for 1.3- and 0.7-mm rotors, respectively, is the primary method to reduce ^{1}H line widths [53]. While faster MAS requires rotors to be smaller in diameter, the higher inherent detection sensitivity of ^{1}H compensates for the smaller sample volume and makes proton-detected experiments attractive. The narrower ^{1}H line widths at fast MAS also open up the possibility to perform multidimensional homonuclear ^{1}H experiments [22], which is of interest in particular when working with unlabelled material. As many cells (bacteria, plants, yeast or others) are difficult to culture in isotopically-labelled media,^{1}H-^{1}H correlation spectra are particularly attractive. Spectral dispersion, however, is typically more limited in a ^{1}H dimension than in a ^{13}C dimension, and the choice of experiment depends on all of these factors [29], as well as the intrinsic dynamics of the sample components. In this respect, INEPT-based experiments proved to be better suited to evidence highly flexible portions of biological solids, while CP-based experiments emphasise more rigid portions [22,41,45,47,49,51,54].

Sensitivity limitations – often the main bottleneck – can also be addressed with optimised hardware. Optimal design of the RF circuit (including the use of double-resonance vs. triple-resonance probes) or the rotor volume (*e.g.* thin-walled vs. normal-walled rotor) can lead to a very substantial sensitivity gain, as investigated recently in a systematic study by Rienstra and co-workers [55]. The optimisation of probe technology has recently made a leap forward with the development of a cryogenically cooled 3.2 mm MAS probe optimised for heteronuclear detection. This probe, henceforth called CPMAS CryoProbe, has been shown to deliver a sensitivity gain of ca. 3 to 4 per milligram of non-soluble and non-crystalline samples of biological assemblies [56]. Moreover, as the rotors used for this probe are larger (ca. 90 µL, or 81 µL with an insert) than those used for a standard 3.2 mm probe (32 µL for standard wall, 46 µL for thin wall), sensitivity enhancements up to a factor of ca. 8 have been reported for multidimensional experiments [56–58].

Here, we investigate different solid-state NMR (ssNMR) methods for obtaining homo- and heteronuclear correlation spectra of bacterial cell walls, and investigate the relative benefits and drawbacks of these methods with respect to detection, sensitivity, and resolution. Using the purified fully hydrated ^{13}C,^{15}N-isotopically labelled cell wall of *Corynebacterium glutamicum*, we compare the sensitivity of ^{13}C-detected experiments obtained with a room-temperature and a CPMAS CryoProbe, and show that sensitivity gains of ca. 8-fold are obtained with the CryoProbe. This allowed us to rapidly collect such experiments on intact fully ^{13}C,^{15}N-isotopically labelled bacterial cells. Moreover, we compare ^{1}H-detected ^{1}H-^{13}C and ^{1}H-^{15}N experiments recorded with either 1.3 mm or 0.7 mm probes. We also apply an INEPT-based H-N-C correlation experiment to detect flexible parts, and show N-C correlations of sugar and peptide components of the bacterial cell wall.

2. Methods

2.1. Cells and cell wall preparation

A 17% glycerol stock of *Corynebacterium glutamicum* ATCC 13032 and of *Mycobacterium smegmatis ΔBlaS* (PM759) are a kind gift of Dr Jean-Emmanuel Hugonnet and Michel Arthur, CRC, Paris. A 1-mL 17% glycerol stock of *C. glutamicum* was used to inoculate 100 mL of M9 minimal medium containing 0.525 g of Na_2HPO_4, 0.3 g of KH_2PO_4, 0.05 g of NaCl, 0.12 g of $MgSO_4$, 11 mg of $CaCl_2$, 12.6 mg of $MnCl_2$, 8.07 mg of $ZnSO_4$, 8.1 mg of $FeCl_3$, 0.1 g of NH_4Cl, 0.2 g of glucose, 1 g of trehalose, 0.2 g of ISOGRO®, and a vitamin cocktail (0.1 mg of pyridoxine, biotin, D-panthothenic acid hemicalcium salt, folic acid, choline chloride, niacinamide, 10 µg of riboflavine, and 0.5 mg of thiamine). This pre-culture is grown at 30 °C and 220 rpm overnight until $OD_{600\ nm}$ reaches more than 6 and used in a 1:10 ratio to inoculate a 1-L culture medium with ^{15}N and ^{13}C-isotopically labelled nitrogen and carbon sources (^{15}N-NH_4Cl,^{13}C-glucose, and ^{13}C,^{15}N-ISOGRO®). After 15 h of culture at 30 °C, cells are pelleted for 20 min at 5000 × g and 4 °C, washed once with fresh medium and frozen until cell wall purification. This protocol typically yields 10 g of cell pellet per liter of culture.

For purification of the cell wall of *C. glutamicum*, cell pellets are resuspended in 15 mL of ice-cold ultra-pure water (resistivity lower than 18.2 MΩ and TOC ≤ 5 ppb) and the suspension is added dropwise into 120 mL of a stirred boiling 5% sodium dodecylsulfate (SDS) solution at 90 °C. The mixture is incubated at 90 °C for an additional 30 min and allowed to slowly cool down to room temperature overnight. The cell wall is recovered by centrifugation at 46,000 × g and 20 °C, washed twice with 20 mL of 1 M NaCl at room temperature, and freed from SDS using 5-to-10 washes with 20 mL of ultra-pure water at 60 °C. After centrifugation and removal of the supernatant, pellets are resuspended in 20 mL of a 100 mM Tris–HCl, 20 mM $MgSO_4$ buffer at pH 7.5. Cell wall samples are then processed successively with a mixture of DNAseI (10 µg/mL) and RNAse (50 µg/mL) for two hours and 100 µg/mL porcine pancreatic trypsin or Pronase E overnight at 37 °C. Enzymes are inactivated by the addition of SDS (4% w/v final concentration) and incubation for 30 min at 80 °C. The cell wall sample is then washed extensively with ultra-pure water until SDS free, as previously. Finally, the sample is incubated for 15 min at 37 °C in 10 mL of 100-mM EDTA at pH 7.0 to remove traces of paramagnetic metals and washed twice with ultra-pure water. After isolation by ultracentrifugation and lyophilization, ≈ 44 mg of *C. glutamicum* cell wall is obtained. The solid is finally resuspended in 600 µL of 50 mM HEPES buffer at pH = 7.0 to pack fully hydrated ^{13}C,^{15}N-isotopically labelled cell wall in the solid-state NMR rotors used in this study.

To prepare the ^{13}C,^{15}N-labelled *M. smegmatis* sample, a 1-mL 17% glycerol stock of cells was innoculated into 100 mL of pre-culture composed of basic M9 medium (without vitamins) containing 1 g/L of ^{15}N-NH_4Cl, 2 g/L ^{13}C-glucose and ^{13}C,^{15}N-Celtone®. This pre-culture was incubated at 37°C and 220 rpm for 84 h until $OD_{600\ nm}$ = 1.5. The pre-culture was used to innocculate a 1-L culture in labelled M9 medium, as previously stated for *C. glutamicum* cells. After incubation at 37 °C and 120 rpm for 84 h, cells were pelleted and stored at −80 °C with 30% DMSO until packing of the 3.2 mm rotor.

2.2. Solid-state NMR sample preparation

A 3.2 mm rotor for the CPMAS CryoProbe (volume 81 µL with an insert for wet samples) was filled with fully hydrated ^{13}C,^{15}N-labelled *C. glutamicum* cell wall (before rehydration of the lyophilized cell wall sample the mass was ca. 44 mg). The fully hydrated cell wall sample was filled into a rotor using a tabletop centrifuge for ca. 1 h at a centrifugal force of 16,000 × g. For the intact cell sample, *M. smegmatis* cells were unfrozen, extensively washed and resuspended in 50 mM HEPES buffer at pH = 7.0, before to be packed into the CPMAS Cryoprobe rotor as for *C. glutamicum* cell wall sample.

For the experiments with the room-temperature 3.2 mm probe, the fully hydrated ^{13}C,^{15}N-isotopically labelled *C. glutamicum* cell wall material was removed from the CryoProbe rotor and centrifuged into a thin-wall 3.2-mm rotor (volume 40 µL). Due to the smaller volume of the rotor compared to the CryoProbe rotor, not all the sample could be filled, and we estimate that the room-temperature thin-walled rotor contained ca. 50% less material than the CryoProbe rotor (corresponding approximately to the ratio of the rotor volumes).

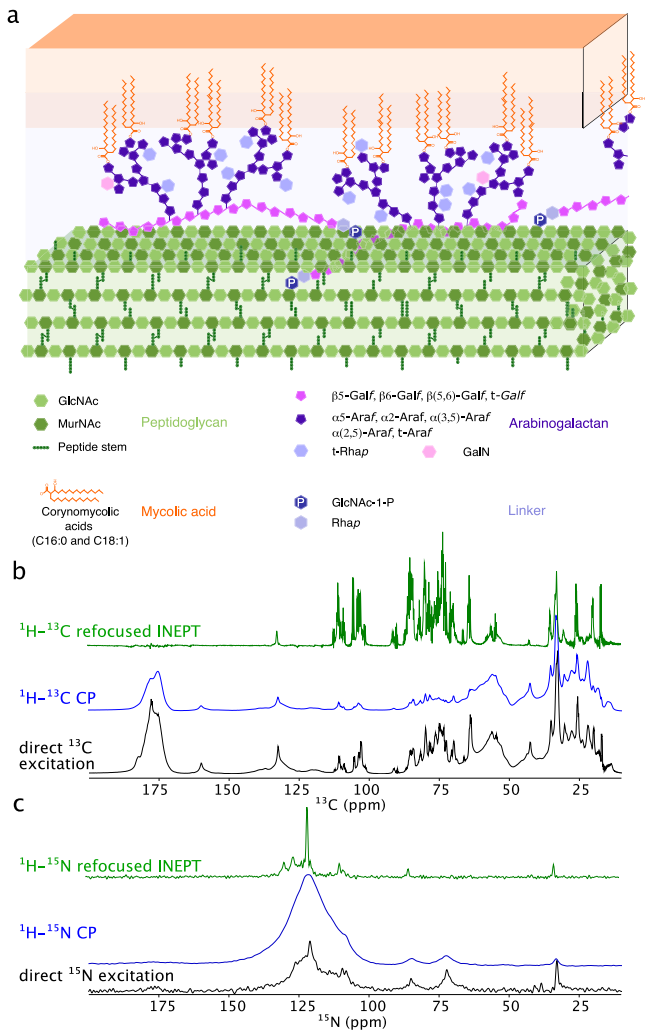

Fig. 1. Architecture and 1D MAS NMR spectra of fully hydrated ^{13}C,^{15}N-labelled *C. glutamicum* isolated cell wall. (a) Schematic organisation of the cell wall. The mAGP complex is composed of peptidoglycan with GlcNAc-MurNAc-peptide motifs in green, covalently linked to an arabinogalactan layer in dark purple and pink, with arabinans esterified by corynomycolic acids in orange. A detailed molecular view is provided in Figure S1. (b) One-dimensional ^{13}C spectra of the cell wall were recorded on the 3.2 mm Efree probe at 15 kHz MAS frequency using 1.89 s relaxation delay and an acquisition time of 29.9 ms. The spectrum with direct ^{13}C excitation was collected with 11,776 scans, while only 8320 scans were used for spectra with ^{1}H-to-^{13}C transfers. The CP duration and INEPT delay were set to 1 and 1.5 ms, respectively. (c)^{15}N spectra of the cell wall were recorded on the 1.3 mm Efree probe at 55.5 kHz MAS frequency using 3.0 s relaxation delay and an acquisition time of 24.9 ms. The spectrum with direct ^{15}N excitation was collected with 38,400 scans, while 38,720 scans were used for spectra with ^{1}H-to-^{15}N transfers. The CP duration and INEPT delay were set to 0.6 and 2.4 ms, respectively.

The 1.3 mm rotor (volume 2.5 μL) and the 0.7 mm rotor (volume 0.6 μL) were filled with a new batch of fullyhydrated ^{13}C,^{15}N-isotopically labelled *C. glutamicum* cell wall using a custom-made ultracentrifuge tool in a SW32 Beckman rotor spinning at ca. 60000 *x* g (20,000 rpm) and 4 °C for 1 h.

2.3. MAS NMR

^{13}C-detected experiments were performed using 3.2 mm MAS probes at 600 MHz ^{1}H Larmor frequency. As indicated in the main text, either a room-temperature Efree probe or a CPMAS CryoProbe were used.^{1}H-detected experiments were performed with room-temperature 1.3 mm (operating at 600 or 950 MHz ^{1}H Larmor frequency) or 0.7 mm (at 950 MHz) probes.

Signal-to-noise ratios for the comparison of the spectra obtained with the CryoProbe and the room-temperature probe (Fig. 3) as well as the spectra obtained with the 1.3 mm and the 0.7 mm probes (Fig. 5) were determined as follows. The spectra were processed with identical parameters (in particular the acquisition times in both dimensions and the apodisation functions), and baseline corrected. To determine the noise level, the intensity at ca. 1000 positions in a region without peaks was extracted, at random positions (not necessarily at extremes). The standard deviation of the intensities at these randomly chosen positions was used as the noise level. The peak heights and this noise level were used to calculate the sensitivity. In comparing sensitivities, differences in the experimental times have been corrected, by multiplication with a factor corresponding to the square root of the ratio of the number of scans. The signal-to-noise ratio was also estimated with the routine implemented in the CCPN software (version 3.1) [59], which is the program used for all spectra analyses. All spectra were processed with the Topspin software (version 4.3). Details on acquisition and processing parameters are provided in supplementary Table S1.

3. Results and discussion

3.1. Heteronuclear NMR investigation of the mAGP complex of C. glutamicum

Fig. 1a shows the architecture of the complex mycoloyl-arabinogalactan-peptidoglycan polymer (mAGP complex) of the *Corynebacterium glutamicum* cell wall. Detailed chemical structures of the essential constituting motifs are shown in Figure S1, according to the current knowledge brought by biochemical fragmentation and combined chromatography, mass spectrometry and solution-state NMR analysis (for a recent review see Houssin et al. [11]). However these approaches may suffer from incomplete solubilisation and artifactual degradation of the constituting components by the rather stringent chemical treatment (concentrated sodium hydroxyde, trifluoro acetic acid and/or hydrofluoric acid). Solid-state NMR of the intact polymer are thus of particular interest to get insights into the structural and dynamical heterogeneity of this biopolymer. Commonly employed experiments in biological magic-angle spinning solid-state NMR are based either on dipolar-coupling transfers, such as cross-polarisation (CP) [60] or dipolar-assisted rotational resonance (DARR [61]), or on *J*-coupling based transfers (INEPT [62]). The efficiency of CP and INEPT transfers in MAS NMR in the presence of molecular motion have been studied in detail [22,41,45,47,49–51,54]. INEPT transfer works well when the coherence life time is long enough for the transfer delays, which mostly occurs when large-amplitude motion on ps-ns time scales average dipolar couplings. For CP transfer to be efficient only low-amplitude motion can be present. In both cases, motions on μs time scales would broaden the lines.

Cell wall 1D ^{13}C CP-NMR of *Mycobacterium smegmatis* and *Mycobacterium abscessus*, two mycobacteria of the same *Corynebacteriales* order than *C. glutamicum*, have been reported very recently on lyophilised extracted mAGP material [12]. In fully hydrated samples, such as the *C. glutamicum* cell wall and the *M. smegmatis* entire bacteria samples of the present study, all components are nevertheless not present in the CP-MAS spectra. For this reason, one-dimensional ^{13}C and ^{15}N spectra in the present study were collected with different excitation schemes (direct excitation, cross-polarisation from ^{1}H, or refocused INEPT from ^{1}H) on the *C. glutamicum* cell wall sample. The comparison of corresponding spectra in Fig. 1 indeed reveals the heterogeneity of dynamics of the different components. Intense ^{13}C resonances in the 125–150 ppm and the 10–50 ppm regions arising from the double bond and aliphatic chains of the lipidic part of mycolic acid, respectively, show up in both INEPT- and CP-type spectra, suggesting that some of the lipidic tails are free in solution, while some other may have a supramolecular organisation in the absence of the other portions of the outer-membrane in this isolated cell wall sample (Fig. 1b). Saccharides

(with ^{13}C resonances in the 100–110 ppm and 60–80 ppm regions for the anomeric carbons and the rest of the sugar carbons, respectively) are exacerbated in the refocused INEPT spectrum, suggesting that most of them are highly flexible in fully hydrated cell walls. Peptides and eventually N-acetylated sugars (160–190, 100–110, and 50–60 ppm regions for carbonyls, anomeric carbons in the sugars and Cα of peptides, respectively) are clearly detected in CP-spectra, suggesting that peptidoglycan might be more rigid.^{15}N spectra reflect the same behaviour with flexible N-acetylated sugars and peptides (100–130/25–50 and 100–150/60–80 ppm regions, respectively) showing intense signals in the refocused INEPT and CP spectra, respectively. Given this heterogeneous behaviour, with intense signals arising from both the CP- and INEPT- based experiments, we used both types of experiments in this study to investigate further the isolated mAGP complex of *C. glutamicum* in native-like fully hydrated samples.

In line with the 1D spectra, two-dimensional ^{13}C-^{13}C correlation spectra recorded at 15 kHz MAS frequency show a different contribution to the signal of the different parts of the *C. glutamicum* mAGP complex (Fig. 2). Signals in the CP-based experiment are mostly from sugar parts and peptide parts of the peptidoglycan component. In addition a fraction of the mycolic acids close to the double bond, that is described as promoting the stacking of the lipidic chains, but also to some extent the galactans of the arabinogalactans and eventually the linker between the peptidoglycan and the arabinogalactan scaffold, are detected in the DARR spectrum of Fig. 2a . We find the 250 ms DARR mixing time to be a good compromise for most resonances, which arise from the raiser rigid peptidoglycan portion of the mAGP complex (Fig. S2) . The *J*-coupling based experiment, on the other hand, shows sharp signals arising mainly from the arabinans and some galactans of the arabinogalactans, most certainly un-cross-linked peptides of the peptidoglycan, and the mycolic acids. Thus, while the same type of motifs contribute to the different spectra, it is assumed that those signals stem from different "layers" of a given type of structure, *e.g.* different parts within the peptidoglycan, or arabinogalactans or mycolic acids. The comparison of the two spectra thus allows to establish that the saccharidic chains and the cross-linked peptides of peptidoglycan in mAGP are rather rigid, as well as some of the galactans, while arabinans and mycolic acids of mAGP are rather flexible in fully hydrated native-like conditions.

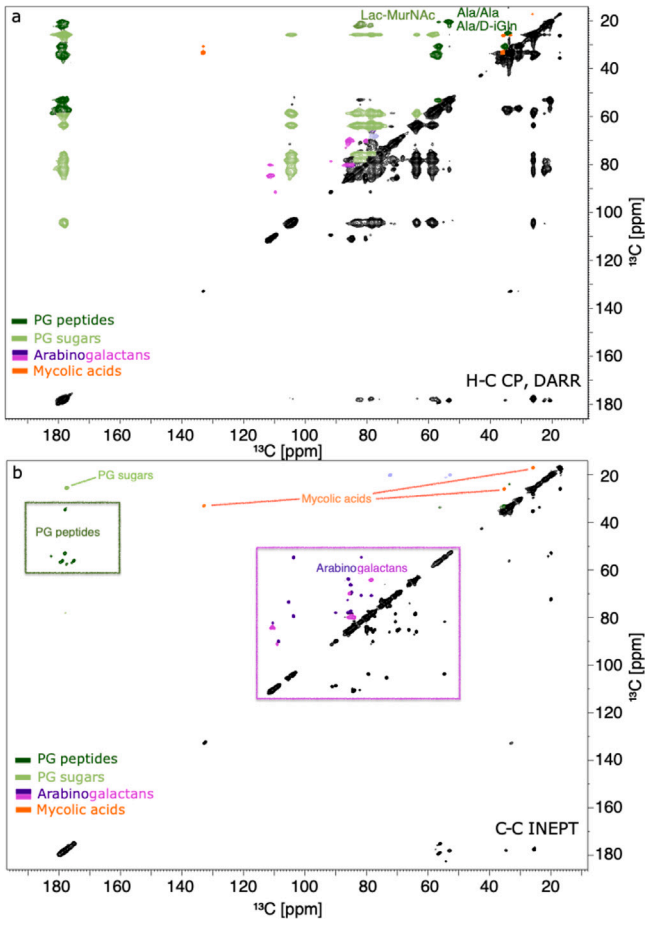

Fig. 2. ^{13}C-detected ^{13}C-^{13}C correlation spectra of fully hydrated ^{13}C,^{15}N-labelled *C. glutamicum* isolated cell wall using either (a) a 1 ms ^{1}H-^{13}C cross-polarisation and DARR transfer or (b) a 1.4 ms ^{1}H-^{13}C refocused INEPT and 1.5 ms ^{13}C-^{13}C refocused INEPT. The DARR spectrum in panel (a) was recorded with 4 scans, a DARR mixing time of 250 ms, acquisition times of 15 and 8.7 ms in the direct and indirect dimensions, respectively, and a recycle delay of 1.7 s using the Efree MAS probe at 14.1 *T* for a total experimental time of 2.5 h. The ^{13}C–^{13}C INEPT spectrum in panel (b) was collected with 4 scans, acquisition times of 20 ms and 8.5 ms in the direct and indirect dimensions, respectively, and a recycle delay of 2.8 s using the CPMAS CryoProbe for a total experimental time of 2.5 h.

3.2. Enhanced sensitivity in ^{13}C detected experiments with a CPMAS CryoProbe

We have investigated the sensitivity benefit that can be obtained with a CPMAS CryoProbe for the 2D ^{13}C-detected experiments. We have recorded these two experiments with the same sample of *C. glutamicum* cell wall, filled either into a rotor compatible with the CPMAS CryoProbe (volume ca. 81 μL) or a thin-walled 3.2 mm rotor for a room-temperature probe (volume ca. 40 μL). A one-scan direct-exitation experiment recorded with the CryoProbe shows very high sensitivity (Fig. 3a). To quantify the gain compared to a room-temperature probe, we investigated the ratio of signal-to-noise ratios obtained for the corresponding cross peaks in 2D spectra (*J*-coupling based spectra in panel b and DARR spectra in panel c). The gain in sensitivity (signal-to-noise per unit time) obtained with the CryoProbe is ca. a factor 8 in both types of experiments. The enhancement is not uniform for all peaks, as shown by the distributions in Fig. 3b,c. We ascribe this observation primarily to somewhat different optimisations of the experiments (each experiment was individually optimised for highest sensitivity), which *e.g.* results in different CP settings. Those settings will impact different peaks differently. Moreover, the distribution of enhancement factors becomes slightly more narrow when taking only peaks which have a higher signal-to-noise ($\geq$ 30 in both spectra; blue data set in Fig. 3).

The observed gains in sensitivity translate to a ca. 64-fold acceleration of the data collection, which is very substantial. Part of this gain can be ascribed to the increased sample amount (ca. a factor of 2), and part of it to the noise reduction in the CryoProbe. Possibly another gain stems from the higher RF field homogeneity. Our findings are in line with other reports of the sensitivity gain from the CPMAS CryoProbe. For protein samples, a gain of ca. 3 for 1D ^{13}C spectra has been reported for different biological assemblies by Hassan et al. [56] and a factor 3.2 for a protein covalently linked to hydroxyapatite [63]. For NCC-type multidimensional spectra a factor of 7–7.7 was found for biomolecules [56]. A factor of 4 to 6 has been found in pharmaceuticals (organic solids) [58].

The improved sensitivity provided by the CPMAS CryoProbe allowed us to obtain a spectrum of intact fully ^{13}C,^{15}N-labelled bacteria (rather than only the mAGP complex of the cell wall). Compared to experiments with isolated (*i.e.*, purified) mAGP, the sample volume contains relatively much less cell wall. Nonetheless, an INEPT-based ^{13}C-^{13}C correlation spectrum of intact *Mycobacterium smegmatis* bacteria could be obtained in 12 h (512 increments, using a recycle delay of 2.8 s; Fig. 4). The study of the impact of antibiotic treatment on intact *Corynebacteria* becomes thus highly amenable at an atomic resolution using this strategy.

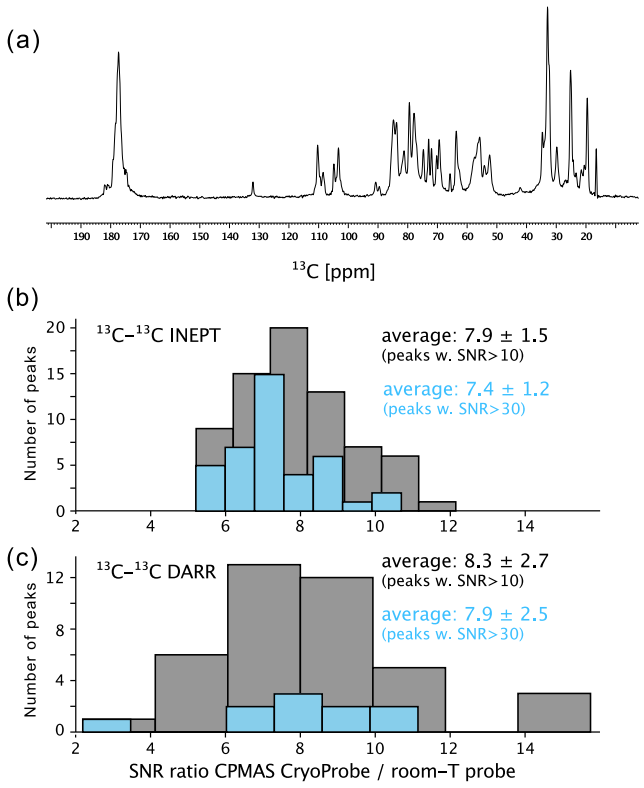

Fig. 3. Sensitivity enhancement of ^{13}C-detected experiments with the CPMAS CryoProbe. (a) Single-pulse direct-excitation ^{13}C spectrum from a single scan. (b) Ratio of signal-to-noise ratios (SNR) obtained for a of fully hydrated ^{13}C,^{15}N-labelled *C. glutamicum* isolated cell wall sample with the CPMAS CryoProbe over the SNR obtained with a 3.2 mm room-temperature Efree probe, from a J-based (INEPT)^{13}C-^{13}C correlation spectrum with direct ^{13}C excitation. (c) Ratio of SNRs in ^{13}C-^{13}C DARR experiments with initial ^{1}H-^{13}C cross-polarisation. For the comparisons only peaks have been used which have a SNR ≥ 10 or 30 with grey or blue histograms, respectively. Average and standard deviation values over the different peaks are also reported with the corresponding colour.

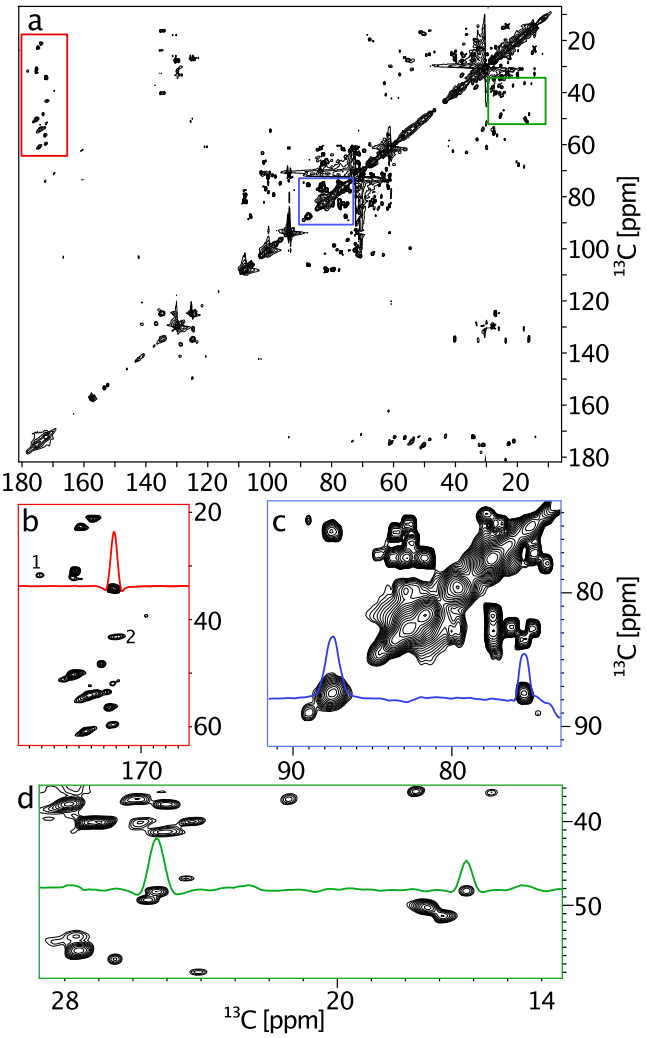

Fig. 4. ^{13}C-excited ^{13}C-^{13}C INEPT spectrum of intact ^{13}C,^{15}N-labelled *Mycobacterium smegmatis* bacteria recorded with the CPMAS CryoProbe in 12 h experimental time (512 increments with 200 ppm spectral width, 8.4 and 19.9 ms acquisition times in the indirect and direct dimensions, respectively; recycle delay 2.8 s; 1.7 ms INEPT delay). Excerpts from the full spectrum (a) at three locations, indicated by coloured boxes, are shown in (b-d), including 1D traces. The signal-to-noise ratios for the five peaks shown in the traces in (b) (intra-peptide stem correlation), (c) (intra-sugar correlations), and (d) (peptide aliphatic region) are ca. 140, 90, 65, 20 and 11 (from left to right). The peaks indicated with "1" and "2" in (b) have S/N ratios of 7 and 12, respectively. In (b-d), the consecutive contour lines are separated by a factor of 1.3 in intensity, while in (a) this factor is 2.

3.3. ^{1}H detected experiments provide complementary insights

An alternative to ^{13}C detection is the ^{1}H detection, best combined with high MAS frequencies to suppress line broadening by second-order and higher-order average-Hamiltonian terms [64]. High MAS frequencies are enabled only by smaller rotors, which comes with smaller sample amount generally leading to lower sensitivity [53]. Figs. 5a and S4 show CP-based hCH spectra of fully hydrated ^{13}C,^{15}N-labelled *C. glutamicum* isolated cell wall samples recorded at 100 kHz MAS with a 0.7 mm probe at 950 MHz ^{1}H Larmor frequency. Despite the high MAS frequency, resonances are fairly broad with only few resolved peaks. Resolution is much better in *J*-coupling based experiments (Fig. 5b) with ^{1}H line widths of the order of 80 to 120 Hz (950 MHz; Fig. 5d). Akin to the *J*-coupling based ^{13}C-^{13}C spectrum of Fig. 2b, the spectrum shows correlations primarily from the flexible arabinogalactans, but also from some of the peptidoglycan peptides and sugars, as well as some of the mycolic acids. The CP and INEPT spectra essentially do not overlap, suggesting that two drastically different portions of the cell wall are sampled by these experiments, the resonances in the CP spectrum remaining unidentifed at this stage.

For the *J*-based experiment, which has higher resolution, we then investigated whether the higher MAS frequency enabled by 0.7 mm rotors leads to significant benefits in resolution, and how the sensitivity compares to 1.3 mm rotor at ca. half the MAS frequency. The probes were not available at the same static magnetic field, and we, thus, compare 600 MHz data with 950 MHz data. Analysis of the signal-to-noise ratios shows that the 1.3 mm (55 kHz MAS, 600 MHz) probe clearly outcompetes the 0.7 mm probe (100 kHz MAS, 950 MHz), by a factor 1.7 (± 0.5). The static magnetic field would, instead, predict a factor of ca. 0.5 for the comparison of 600 vs 950 MHz ($B_0^{3/2}$ correction [65]). Although this comparison is approximate and the details depend on the probe design, which may differ at different static magnetic field strengths, this data suggests that the overall sensitivity of a 1.3 mm rotor is ca. 3.4 times higher than that of a 0.7 mm rotor. This ratio approaches the ratio of the rotor volumes (2.5 vs 0.59 μL).

Lastly, we recorded ^{1}H-^{15}N correlation spectra with refocused INEPT and CP transfers on the fully hydrated ^{13}C,^{15}N-labelled *C. glutamicum* isolated cell wall sample. Nitrogens are exclusively located in the peptide and N-acetylated sugars of peptidoglycan as well as on the phosphorylated N-acetylglucosamine of the linker and potentially the galactosamine decorating the arabinogalactans (Figure S1). The 1D ^{15}N (Fig. 1c) and 2D hNH (Fig. 6a) spectra obtained with CP transfer are very broad and hardly useful. We cannot determine with certainty the origin of the broad lines, but see several possible reasons.

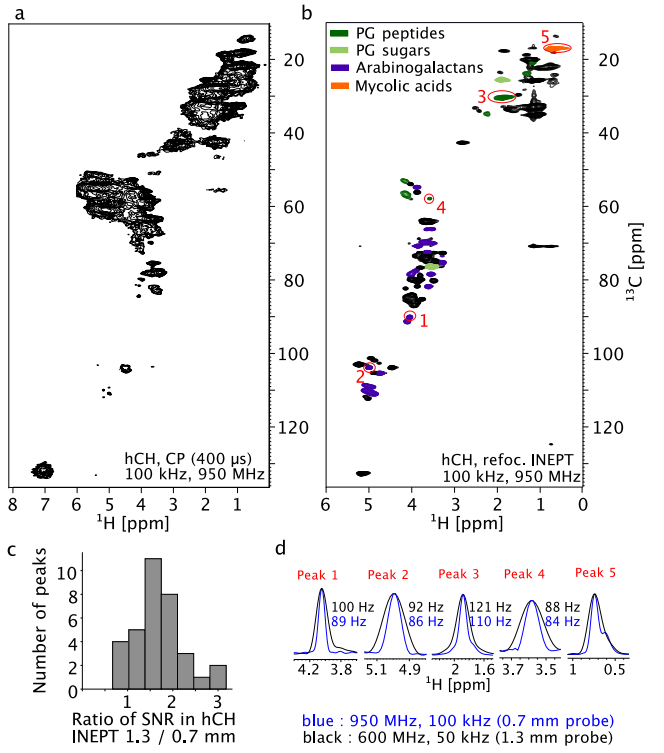

Fig. 5. ^{1}H-detected hCH correlation spectra of fully hydrated ^{13}C,^{15}N-labelled *C. glutamicum* isolated cell wall. (a) Dipolar-coupling based out-and-back hCH experiment, recorded at a MAS frequency of 100 kHz (0.7 mm rotor) and a ^{1}H Larmor frequency of 950 MHz, using an CP contact time of 800 µs for ^{1}H and ^{13}C RF fields of 30 and 120 kHz, respectively, an acquisition time in the direct and indirect dimension of 15 and 12 ms, respectively, a recycle delay of 0.89 s for a total experimental time of 8.5 h. (b) J-coupling based out-and-back hCH experiment with refocused INEPT transfers collected at 100 kHz MAS, on a spectrometer operating at 950 MHz ^{1}H frequency, using an INEPT transfer delay of 1.1 ms, acquisition times in the direct and indirect dimension of 15 and 12 ms, respectively, a recycle delay of 0.9 s for a total experimental time of 4.5 h. (c) Ratio of signal-to-noise per unit time obtained in INEPT spectra at 600 MHz (55 kHz) and 950 MHz (100 kHz). (d) 1D traces of cross peaks in the INEPT experiments, indicating the full-width at half height in Hz, for spectra collected at 100 kHz or 55 kHz MAS using 0.7 mm and 1.3 mm room temperature probes, respectively.

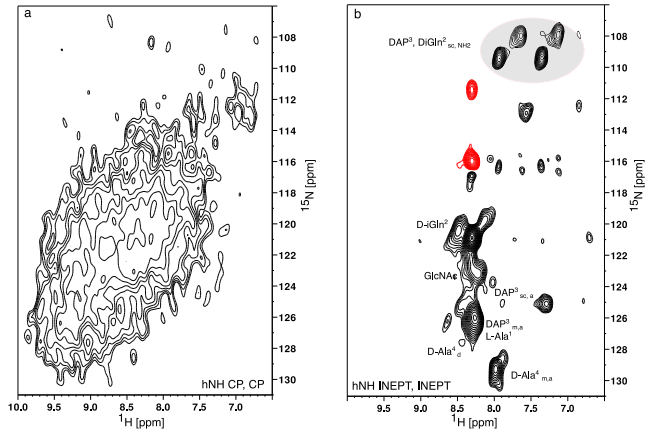

Fig. 6. ^{1}H-^{15}N correlation spectra of fully hydrated ^{13}C,^{15}N-labelled *C. glutamicum* isolated cell wall recorded at 950 MHz and 100 kHz MAS using out-and-back experiments with either (a) CP transfer or (b) refocused INEPT. CP and INEPT data were collected with the same 15 and 13 ms acquisition times in the direct and indirect dimensions, respectively. Relaxation delay was set to 0.9 s. The CP experiment was collected with 48 scans and a cross-polarisation time of 600 µs. The INEPT experiment was collected with 400 scans and an INEPT transfer delay of 1.9 ms. For a comparison equivalent data collected at 600 MHz with a 1.3 mm probe are depicted in Figure S5. Signals in red correspond to negative peaks that are folded back in the ^{15}N dimension.

Interaction of the peptide parts with glycan stems may lead to (static) conformational disorder. The fact that there is also some chemical heterogeneity in the glycan strands and peptide stems may add to this variety of environments for the peptides. The chemical shifts of amide moieties are particularly sensitive to hydrogen bonding geometry, and even small differences in hydrogen bonding geometry result in large alterations of ^{1}H frequencies [66]. Moreover, the presence of motion of the peptide moieties may furthermore lead to the observed line broadening, either through the fluctuation of dipolar coupling and CSA (particularly on µs time scales) or through modulation of the isotropic chemical shift (particularly when it occurs on ms time scales). This effect seems to be more pronounced for ^{1}H-^{15}N spectra than for ^{1}H-^{13}C, as reported for other biomolecular systems. As an example, it has been reported that ^{1}H-^{15}N line widths and relaxation in crystalline ubiquitin differ significantly between three different crystal forms, and line broadening is observed particularly in a crystal form that undergoes molecular rocking within the crystal [67]. However, in the same set of three crystal forms, the side chain ^{1}H-^{13}C signals hardly differ in line widths. In amyloid fibrils it is also commonly observed that ^{1}H-^{15}N line widths are large, significantly more so than in crystalline proteins, and often significantly more so than aliphatic ^{1}H or ^{13}C line widths (see *e.g.* [68,69]). Nonetheless, the very broad ^{1}H-^{15}N spectrum of Fig. 6 indicates that there must be an additional contribution.

We cannot exclude that some proteins that are particularly strongly bound to the cell wall are present in the sample, even though our samples were treated with proteases and extensively washed to remove bound proteins. The amide moieties of proteins would then be observed particularly in CP-based experiments, as they are tightly bound and thus rigid [28]. As the sensitivity of the ^{1}H-^{15}N signal is also rather low, the presence of protein at low abundance is a plausible explanation for the observed spectrum.

The 2D INEPT-based hNH spectrum (Fig. 6b) shows much better resolution with ^{1}H line widths of the order of 80 Hz. These resonances have been tentatively assigned based on previous knowledge on peptidoglycan from other strains [22]. Additional resonances are detected and would require more investigation that is beyond the scope of the present study. This data shows that for the highly flexible parts well-resolved nitrogen correlation spectra can be obtained. However, the information content and resolution are restricted by narrow ^{1}H dispersion, where most peaks fall within ca. 0.5 ppm.

3.4. ^{15}N-^{13}C 2D/3D experiments of flexible segments

Encouraged by the good resolution in *J*-based ^{15}N correlation spectra and to increase further the resolution and information content of nitrogen correlation spectra, we implemented different variants of 2D ^{15}N-^{13}C and 3D^{1}H-^{15}N-^{13}C experiments based on INEPT transfers. Fig. 7a shows the pulse sequence for a proton-excited, carbon-detected hNCO experiment, and panel b shows a straightforward extension by a carbon–carbon refocused INEPT element.

The hNCO and hNCA correlation spectra (Fig. 7c, d) show signals from sugars, in particular N-acetylglucosamine (GlcNAc) and or N-acetylmuramic acid (MurNAc), as well as backbone or side-chain (sc) amide resonances of the peptide stems of peptidogycan (DAP, Ala and or D-iGln). To push further the assignment of these resonances, we have recorded additional hNCOCX and hNCACX experiments using the pulse sequence shown in Fig. 7b. Only one additional cross peak was observed from the transfer between the carbonyl of the amide side-chain resonance and the adjacent C_{α} or C_{ϵ} carbon of D-iGln^{2} or DAP^{3}, respectively of a peptide stem (Figure S6).

4. Conclusions

We have investigated here different ways to collect correlation spectra on ^{13}C,^{15}N-labelled isolated cell-wall and intact bacteria samples from *Corynebacteriales*. A major finding is that the CPMAS CryoProbe,

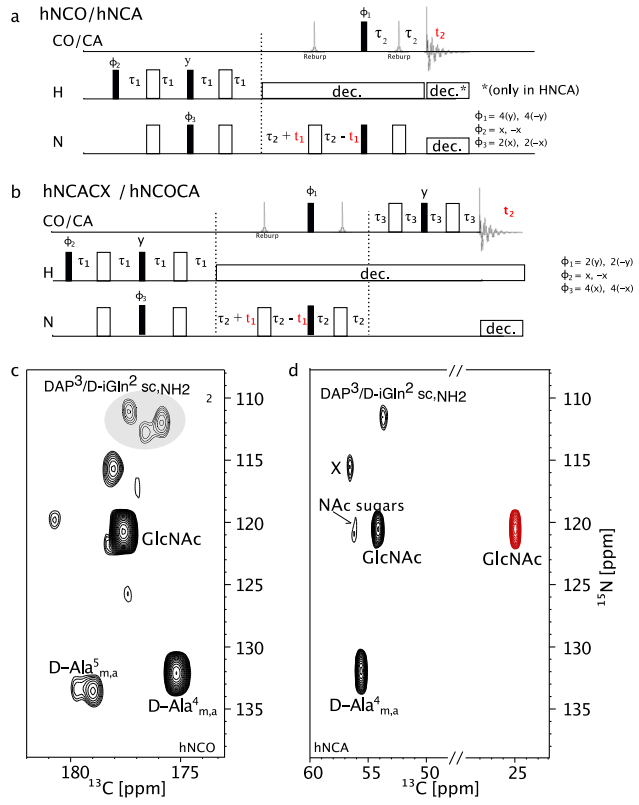

Fig. 7. Detecting flexible parts of fully hydrated ^{13}C,^{15}N-labelled *C. glutamicum* isolated cell wall with INEPT-based H-N-C correlation experiments. (a) Pulse sequences for hNCO and hNCA experiments (these two differ only in the choice of the ^{13}C carrier position) and (b) the hNCC experiments. All pulse phases are x unless indicated otherwise. Filled and open rectangles denote the 90° and 180° pulses. Decoupling was achieved with the WALTZ-16 scheme applied at 3 kHz (^{15}N) or 5 kHz (^{1}H). (c) hNCO and (d) hNCA spectra obtained with the isolated *S. glutamicum* cell wall sample at 15 kHz MAS frequency (3.2 mm rotor, 600 MHz). The experimental durations were 2 h 50 min (hCONH) and 10 h (hCANH) (further acquisition and processing details are specified in Table S1).

applied to this type of sample, provides a large (ca. 8-fold) sensitivity increase over the use of a thin-walled rotor used in a room-temperature probe. We find that for proton-detected spectra, the 1.3 mm rotors provide superior sensitivity compared to 0.7 mm rotors in ^{1}H-^{13}C INEPT-based correlation experiments, which we ascribe to the intrinsic flexibility of some peptide stems of the peptidoglycan, arabinogalactans, and some portions of the mycolic acids, which renders ultra-fast MAS unnecessary. CP-based experiments with ^{1}H detection suffer from rather large line widths. In particular, ^{1}H-^{15}N correlation spectra show very broad lines, presumably due to sample heterogeneity, which render them practically hardly useful. In INEPT-based hNH experiments, however, multiple well-resolved sites were detected from amide resonances of both peptide stems and N-acetylated sugars from the peptidoglycan of the isolated cell wall (mAGP complex) of *C. glutamicum*. Lastly, we find that for the flexible parts INEPT transfers are also efficient for ^{15}N-^{13}C transfers, despite the small couplings (of the order of 10–15 Hz). These N-C correlation experiments may be useful also for other highly flexible components of cellular assemblies.

CRediT authorship contribution statement

Alicia Vallet: Investigation. **Isabel Ayala:** Investigation. **Barbara Perrone:** Resources, Methodology, Investigation. **Alia Hassan:** Resources, Methodology, Investigation. **Jean-Pierre Simorre:** Writing – review & editing, Conceptualization. **Catherine Bougault:** Writing – original draft, Resources, Methodology, Investigation, Conceptualization. **Paul Schanda:** Writing – original draft, Methodology, Investigation, Conceptualization.

Declaration of competing interest

The authors declare that they have no known competing financial interests or personal relationships that could have appeared to influence the work reported in this paper.

Data availability

The raw data of all spectra (Bruker format), the pulse sequences (Bruker language) and the peaks lists and scripts for the analysis of the signal-to-noise ratios (Fig. 3) have been deposited at the IST Austria Research Explorer under the doi:10.15479/AT:ISTA:17042 (https://research-explorer.ista.ac.at/record/17042).

Acknowledgements

This research was supported by the French Agence Nationale de la Recherche (ANR-16-CE11-0030-12, TransPepNMR). This work used the platforms of the Grenoble Instruct-ERIC center (ISBG; UAR 3518 CNRS-CEA-UGA-EMBL) within the Grenoble Partnership for Structural Biology (PSB), supported by FRISBI, France (ANR-10-INBS-0005-02) and GRAL, financed within the University Grenoble Alpes graduate school (Ecoles Universitaires de Recherche), CBH-EUR-GS (ANR-17-EURE-0003). Financial support from the IR INFRANALYTICS FR2054 for conducting the research and intramural funding by the Institute of Science and Technology Austria (ISTA) are gratefully acknowledged.

Appendix A. Supplementary data

Supplementary material related to this article can be found online at https://doi.org/10.1016/j.jmr.2024.107708.

References

[1] T.J. Silhavy, D. Kahne, S. Walker, The bacterial cell envelope, Cold Spring Harb. Perspect. Biol. 2 (5) (2010) a000414.
[2] S.M. Batt, K.A. Abrahams, G.S. Besra, Top five unanswered questions in bacterial cell surface research, Cell Surf. (2024) 100122.
[3] D.J. Cosgrove, Growth of the plant cell wall, Nature Rev. Mol. Cell Biol. 6 (11) (2005) 850–861.
[4] W. Boerjan, V. Burlat, D.J. Cosgrove, C. Dunand, P. Dupree, K.T. Haas, G. Ingram, E. Jamet, S. Moussu, A. Peaucelle, et al., Top five unanswered questions in plant cell surface research, Cell Surf. (2024) 100121.
[5] K.J. Niklas, E.D. Cobb, A.J. Matas, The evolution of hydrophobic cell wall biopolymers: from algae to angiosperms, J. Exp. Bot. 68 (19) (2017) 5261–5269.
[6] N.A.R. Gow, J.P. Latge, C.A. Munro, The fungal cell wall: structure, biosynthesis, and function, Microbiol. Spectr. 5 (3) (2017) 10–1128.
[7] N.A.R. Gow, A. Casadevall, W. Fang, Top five unanswered questions in fungal cell surface research, Cell Surf. 10 (2023) 100114.
[8] K.A. Abrahams, G.S. Besra, Mycobacterial cell wall biosynthesis: a multifaceted antibiotic target, Parasitology 145 (2018) 116–133.
[9] M. Jankute, J.A.G. Cox, J. Harrison, G.S. Besra, Assembly of the mycobacterial cell wall, Annu. Rev. Microbiol. 69 (2015) 405–423.
[10] C.L. Dulberger, E.J. Rubin, C.C. Boutte, The mycobacterial cell envelope — a moving target, Nat. Rev. Microbiol. 18 (2020) 47–59, http://dx.doi.org/10.1038/s41579-019-0273-7.
[11] C. Houssin, C. de Sousa d'Auria, F. Constantinesco, C. Dietrich, C. Labarre, N. Bayan, Architecture and biogenesis of the cell envelope of *Corynebacterium glutamicum*, in: Corynebacterium Glutamicum: Biology and Biotechnology, Springer, 2020, pp. 25–60.
[12] X. Liu, J. Brčić, G.H. Cassell, L. Cegelski, CPMAS NMR platform for direct compositional analysis of mycobacterial cell-wall complexes and whole cells, J. Magn. Reson Open 16 (2023) 100127.
[13] J.A.H. Romaniuk, L. Cegelski, Bacterial cell wall composition and the influence of antibiotics by cell-wall and whole-cell NMR, Philos. Trans. R. Soc. B 370 (1679) (2015) 20150024.
[14] M. Daffé, M. Mcneil, P.J. Brennan, Major structural features of the cell wall arabinogalactans of Mycobacterium, Rhodococcus, and Nocardia spp, Carbohydr. Res. 249 (1993) 383–398.

[15] L.J. Alderwick, H.L. Birch, K. Krumbach, M. Bott, L. Eggeling, G.S. Besra, Aftd functions as an $\alpha(1\rightarrow5)$ arabinofuranosyltransferase involved in the biosynthesis of the mycobacterial cell wall core, Cell Surf. 1 (2018) 2–14.

[16] H.L. Birch, L.J. Alderwick, D. Rittmann, K. Krumbach, H. Etterich, A. Grzegorzewicz, M.R. McNeil, L. Eggeling, G.S. Besra, Identification of a terminal rhamnopyranosyltransferase (RptA) involved in *Corynebacterium glutamicum* cell wall biosynthesis, J. Bacteriol. 191 (2009) 4879–4887, http://dx.doi.org/10.1128/JB.00296-09.

[17] N.S. Shenouda, Y. Pail, J. Schaefer, G.E. Wilson, A simple solid-state NMR method for determining peptidoglycan crosslinking in *Bacillus subtilis*, Biochim. Biophys. Acta 16 (1996) 217–220.

[18] S.J. Kim, J. Chang, M. Singh, Peptidoglycan architecture of Gram-positive bacteria by solid-state NMR, Biochim. Biophys. Acta 1848 (2015) 350–362.

[19] J.A.H. Romaniuk, L. Cegelski, Peptidoglycan and teichoic acid levels and alterations in *S. aureus* by cell-wall and whole-cell nuclear magnetic resonance, Biochemistry 57 (2018) 3966–3975.

[20] M. Renault, R.T.V. Boxtel, M.P. Bos, J.A. Post, J. Tommassen, M. Baldus, Cellular solid-state nuclear magnetic resonance spectroscopy, Proc. Natl. Acad. Sci. 109 (2012).

[21] T. Kern, S. Hediger, P. Müller, C. Giustini, B. Joris, C. Bougault, W. Vollmer, J.P. Simorre, Toward the characterization of peptidoglycan structure and protein –peptidoglycan interactions by solid-state NMR spectroscopy, J. Am. Chem. Soc. 130 (17) (2008) 5618–5619, http://dx.doi.org/10.1021/ja7108135.

[22] C. Bougault, I. Ayala, W. Vollmer, J.P. Simorre, P. Schanda, Studying intact bacterial peptidoglycan by proton-detected NMR spectroscopy at 100 kHz MAS frequency, J. Struct. Biol. 206 (1) (2019) 66–72.

[23] Y. Pan, N.S. Shenouda, G.E. Wilson, J. Schaefer, Cross-links in cell walls of *Bacillus subtilis* by Rotational-Echo DOuble-Resonance NMR, J. Biol. Chem. 268 (1993) 18692–18695.

[24] S. Sharif, S.J. Kim, H. Labischinski, J. Chen, J. Schaefer, Uniformity of glycyl bridge lengths in the mature cell walls of fem mutants of methicillin-resistant *Staphylococcus aureus*, J. Bacteriol. 195 (2013) 1421–1427, http://dx.doi.org/10.1128/JB.01471-12.

[25] J.A.H. Romaniuk, L. Cegelski, Bacterial cell wall composition and the influence of antibiotics by cell-wall and whole-cell NMR, Philos. Trans. R. Soc. B 370 (2015) 20150024.

[26] G. Tong, Y. Pan, H. Dong, R. Pryor, G.E. Wilson, J. Schaefer, Structure and dynamics of pentaglycyl bridges in the cell walls of staphylococcus aureus by 13 C- 15 N REDOR NMR, Biochemistry 36 (1997) 9859–9866, https://pubs.acs.org/doi/10.1021/bi970495d.

[27] T. Kern, M. Giffard, S. Hediger, A. Amoroso, C. Giustini, N.K. Bui, B. Joris, C. Bougault, W. Vollmer, J.P. Simorre, Dynamics characterization of fully hydrated bacterial cell walls by solid-state NMR: Evidence for cooperative binding of metal ions, J. Am. Chem. Soc. 132 (31) (2010) 10911–10919.

[28] P. Schanda, S. Triboulet, C. Laguri, C.M. Bougault, I. Ayala, M. Callon, M. Arthur, J.P. Simorre, Atomic model of a cell-wall cross-linking enzyme in complex with an intact bacterial peptidoglycan, J. Am. Chem. Soc. 136 (2014) 17852–17860.

[29] J.E. Kelly, C. Chrissian, R.E. Stark, Tailoring NMR experiments for structural characterization of amorphous biological solids: A practical guide, Solid State Nucl. Magn. Reson. 109 (2020) 101686.

[30] W. Zhao, A. Kirui, F. Deligey, F. Mentink-Vigier, Y. Zhou, B. Zhang, T. Wang, Solid-state NMR of unlabeled plant cell walls: high-resolution structural analysis without isotopic enrichment, Biotechnol. Biofuels 14 (2021) 1–14.

[31] A. Poulhazan, M.C.D. Widanage, A. Muszyński, A.A. Arnold, D.E. Warschawski, P. Azadi, I. Marcotte, T. Wang, Identification and quantification of glycans in whole cells: Architecture of microalgal polysaccharides described by solid-state nuclear magnetic resonance, J. Am. Chem. Soc. 143 (2021) 19374–19388, http://dx.doi.org/10.1021/jacs.1c07429.

[32] A.N. Smith, R. Harrabi, T. Halbritter, D. Lee, F. Aussenac, P.C.A. van der Wel, S. Hediger, S.T. Sigurdsson, G. De Paëpe, Fast magic angle spinning for the characterization of milligram quantities of organic and biological solids at natural isotopic abundance by 13C–13C correlation DNP-enhanced NMR, Solid State Nucl. Magn. Reson. 123 (2023) 101850.

[33] I. Goldberga, R. Li, W.Y. Chow, D.G. Reid, U. Bashtanova, R. Rajan, A. Puszkarska, H. Oschkinat, M.J. Duer, Detection of nucleic acids and other low abundance components in native bone and osteosarcoma extracellular matrix by isotope enrichment and DNP-enhanced NMR, RSC Adv. 9 (46) (2019) 26686–26690.

[34] H. Takahashi, I. Ayala, M. Bardet, G. De Paëpe, J.P. Simorre, S. Hediger, Solid-state NMR on bacterial cells: selective cell wall signal enhancement and resolution improvement using dynamic nuclear polarization, J. Am. Chem. Soc. 135 (13) (2013) 5105–5110.

[35] S. Narasimhan, C. Pinto, A. Lucini Paioni, J. van der Zwan, G.E. Folkers, M. Baldus, Characterizing proteins in a native bacterial environment using solid-state NMR spectroscopy, Nat. Protoc. 16 (2) (2021) 893–918.

[36] J.E. Kent, B.E. Ackermann, G.T. Debelouchina, F.M. Marassi, Dynamic nuclear polarization illuminates key protein–lipid interactions in the native bacterial cell envelope, Biochemistry 62 (15) (2023) 2252–2256.

[37] A. Chakraborty, F. Deligey, J. Quach, F. Mentink-Vigier, P. Wang, T. Wang, Biomolecular complex viewed by dynamic nuclear polarization solid-state NMR spectroscopy, Biochem. Soc. Trans. 48 (3) (2020) 1089–1099.

[38] W.Y. Chow, G. De Paëpe, S. Hediger, Biomolecular and biological applications of solid-state NMR with dynamic nuclear polarization enhancement, Chem. Rev. 122 (10) (2022) 9795–9847.

[39] D. Beriashvili, J. Zhou, Y. Liu, G.E. Folkers, M. Baldus, Cellular applications of DNP solid-state NMR–state of the art and a look to the future, Chem. Eur. J. (2024) e202400323.

[40] N. Ghassemi, A. Poulhazan, F. Deligey, F. Mentink-Vigier, I. Marcotte, T. Wang, Solid-state NMR investigations of extracellular matrixes and cell walls of algae, bacteria, fungi, and plants, Chem. Rev. 122 (10) (2021) 10036–10086.

[41] W. Zhao, F. Deligey, S.C. Shekar, F. Mentink-Vigier, T. Wang, Current limitations of solid-state NMR in carbohydrate and cell wall research, J. Magn. Reson. 341 (2022) 107263.

[42] L. Cegelski, R.D. O'Connor, D. Stueber, M. Singh, B. Poliks, J. Schaefer, Plant cell-wall cross-links by REDOR NMR spectroscopy, J. Am. Chem. Soc. 132 (45) (2010) 16052–16057.

[43] T. Wang, Y.B. Park, M.a. Caporini, M. Rosay, L. Zhong, D.J. Cosgrove, M. Hong, Sensitivity-enhanced solid-state NMR detection of expansin's target in plant cell walls, Proc. Natl. Acad. Sci. USA 110 (41) (2013) 16444–16449.

[44] T. Wang, P. Phyo, M. Hong, Multidimensional solid-state NMR spectroscopy of plant cell walls, Solid State Nucl. Magn. Reson. 78 (2016) 56–63.

[45] A.A. Arnold, J.P. Bourgouin, B. Genard, D.E. Warschawski, R. Tremblay, I. Marcotte, Whole cell solid-state NMR study of chlamydomonas reinhardtii microalgae, J. Biomol. NMR 70 (2018) 123–131.

[46] G. Lamon, A. Lends, I. Valsecchi, S.S.W. Wong, V. Duprès, F. Lafont, J. Tolchard, C. Schmitt, A. Mallet, A. Grélard, et al., Solid-state NMR molecular snapshots of Aspergillus fumigatus cell wall architecture during a conidial morphotype transition, Proc. Natl. Acad. Sci. 120 (6) (2023) e2212003120.

[47] L.D. Fernando, Y. Pérez-Llano, M.C. Dickwella Widanage, A. Jacob, L. Martínez-Ávila, A.S. Lipton, N. Gunde-Cimerman, J.P. Latgé, R.A. Batista-García, T. Wang, Structural adaptation of fungal cell wall in hypersaline environment, Nature Commun. 14 (1) (2023) 7082.

[48] C. Reichhardt, L. Cegelski, Solid-state NMR for bacterial biofilms, Mol. Phys. 112 (7) (2014) 887–894.

[49] Y. Xue, C. Yu, H. Ouyang, J. Huang, X. Kang, Uncovering the molecular composition and architecture of the bacillus subtilis biofilm via solid-state NMR spectroscopy, J. Am. Chem. Soc. (2024) 11906–11923.

[50] K. Aebischer, M. Ernst, INEPT and CP transfer efficiencies of dynamic systems in MAS solid-state NMR, J. Magn. Reson. 359 (2024) 107617.

[51] C.H. Byeon, T. Kinney, H. Saricayir, S. Srinivasa, M.K. Wells, W. Kim, Ü. Akbey, Tapping into the native pseudomonas bacterial biofilm structure by high-resolution multidimensional solid-state NMR, J. Magn. Reson. 357 (2023) 107587.

[52] S. Bahri, A. Safeer, A. Adler, H. Smedes, H. van Ingen, M. Baldus, 1H-detected characterization of carbon–carbon networks in highly flexible protonated biomolecules using MAS NMR, J. Biomol. NMR 77 (3) (2023) 111–119.

[53] T. Le Marchand, T. Schubeis, M. Bonaccorsi, P. Paluch, D. Lalli, A.J. Pell, L.B. Andreas, K. Jaudzems, J. Stanek, G. Pintacuda, ^{1}H-detected biomolecular NMR under fast magic-angle spinning, Chem. Rev. 122 (10) (2022) 9943–10018.

[54] P. Duan, M. Hong, Selective detection of intermediate-amplitude motion by solid-state NMR, J. Phys. Chem. B 10 (2024) 2293–2303.

[55] C. Rienstra, R. Han, C.G. Borcik, S. Wang, O.A. Warmuth, K. Geohring, C. Mullen, M. Incitti, J.A. Stringer, Solid-state NMR ^{13}C sensitivity at high magnetic field, 2023, Available at SSRN 4603435.

[56] A. Hassan, C.M. Quinn, J. Struppe, I.V. Sergeyev, C. Zhang, C. Guo, B. Runge, T. Theint, H.H. Dao, C.P. Jaroniec, M. Berbon, A. Lends, B. Habenstein, A. Loquet, R. Kuemmerle, B. Perrone, A.M. Gronenborn, T. Polenova, Sensitivity boosts by the CPMAS CryoProbe for challenging biological assemblies, J. Magn. Reson. 311 (2020) 106680.

[57] J. Shen, V. Terskikh, J. Struppe, A. Hassan, M. Monette, I. Hung, Z. Gan, A. Brinkmann, G. Wu, Solid-state 17 o NMR study of α-d-glucose: exploring new frontiers in isotopic labeling, sensitivity enhancement, and NMR crystallography, Chem. Sci. 13 (9) (2022) 2591–2603.

[58] Y. Du, J. Struppe, B. Perrone, A. Hassan, A. Codina, Y. Su, Efficient analysis of pharmaceutical drug substances and products using a solid-state NMR CryoProbe, Analyst 148 (4) (2023) 724–734.

[59] S.P. Skinner, R.H. Fogh, W. Boucher, T.J. Ragan, L.G. Mureddu, G.W. Vuister, CcpNmr AnalysisAssign: a flexible platform for integrated NMR analysis, J. Biomol. NMR 66 (2016) 111–124.

[60] A. Pines, M.G. Gibby, J.S. Waugh, Proton-enhanced NMR of dilute spins in solids, J. Chem. Phys. 59 (2) (1973) 569–590.

[61] K. Takegoshi, S. Nakamura, T. Terao, C-13-H-1 dipolar-assisted rotational resonance in magic-angle spinning NMR, Chem. Phys. Lett. 344 (5–6) (2001) 631–637.

[62] G.A. Morris, R. Freeman, Enhancement of nuclear magnetic resonance signals by polarization transfer, J. Am. Chem. Soc. 101 (3) (1979) 760–762.

[63] T. Gopinath, K. Shin, Y. Tian, W. Im, J. Struppe, B. Perrone, A. Hassan, F.M. Marassi, Solid-state NMR MAS CryoProbe enables structural studies of human blood protein vitronectin bound to hydroxyapatite, J. Struct. Biol. 216 (1) (2024) 108061.

[64] M. Chávez, T. Wiegand, A.A. Malär, B.H. Meier, M. Ernst, Residual dipolar line width in magic-angle spinning proton solid-state NMR, Magn. Reson. 2 (2021) 499–509.

[65] J. Cavanagh, W.J. Fairbrother, A. Palmer III, N.J. Skelton, Protein NMR Spectroscopy, 2nd Edition Principles and Practice, Academic Press, Burlington, San Diego, London, 2007.
[66] L.L. Parker, A.R. Houk, J.H. Jensen, Cooperative hydrogen bonding effects are key determinants of backbone amide proton chemical shifts in proteins, J. Am. Chem. Soc. 128 (30) (2006) 9863–9872.
[67] P. Ma, Y. Xue, N. Coquelle, J.D. Haller, T. Yuwen, I. Ayala, O. Mikhailovskii, D. Willbold, J.p. Colletier, N.R. Skrynnikov, P. Schanda, Observing the overall rocking motion of a protein in a crystal, Nature Commun. 6 (2015) 8361.
[68] J. Stanek, L.B. Andreas, K. Jaudzems, D. Cala, D. Lalli, A. Bertarello, T. Schubeis, I. Akopjana, S. Kotelovica, K. Tars, A. Pica, S. Leone, D. Picone, X. Zhi-Qiang, N.E. Dixon, D. Martinez, M. Berbon, N. El Mammeri, A. Noubhani, S. Saupe, B. Habenstein, A. Loquet, G. Pintacuda, NMR spectroscopic assignment of backbone and side-chain protons in fully protonated proteins: Microcrystals, sedimented assemblies, and amyloid fibrils, Angew. Chem. Int. Edn 55 (50) (2016) 15504–15509.
[69] A.A. Smith, E. Testori, R. Cadalbert, B.H. Meier, M. Ernst, Characterization of fibril dynamics on three timescales by solid-state NMR, J. Biomol. NMR 65 (3–4) (2016) 171–191.